TU Delft

Delft University of Technology

Document Version
Final published version

Licence
Dutch Copyright Act (Article 25fa)

Citation (APA)
Zuo, Y., Göbel, L., Yliniemi, J., Provis, J. L., & Ye, G. (2026). Modelling and Simulation of Alkali-Activated Materials. In G. Ye, & F. Dehn (Eds.), *Mechanical Properties of Alkali-Activated Materials: State-of-the-Art Report of the RILEM Technical Committee 294-MPA* (pp. 135-159). (RILEM State-of-the-Art Reports; Vol. 46). Springer. https://doi.org/10.1007/978-3-032-07116-3_5

Important note
To cite this publication, please use the final published version (if applicable).
Please check the document version above.

Copyright
In case the licence states “Dutch Copyright Act (Article 25fa)”, this publication was made available Green Open Access via the TU Delft Institutional Repository pursuant to Dutch Copyright Act (Article 25fa, the Taverne amendment). This provision does not affect copyright ownership.
Unless copyright is transferred by contract or statute, it remains with the copyright holder.

Sharing and reuse
Other than for strictly personal use, it is not permitted to download, forward or distribute the text or part of it, without the consent of the author(s) and/or copyright holder(s), unless the work is under an open content license such as Creative Commons.

Takedown policy
Please contact us and provide details if you believe this document breaches copyrights.
We will remove access to the work immediately and investigate your claim.

This work is downloaded from Delft University of Technology.

Modelling and Simulation of Alkali-Activated Materials



Yibing Zuo, Luise Göbel, Juho Yliniemi, John L. Provis, and Guang Ye

Abstract Numerical models are helpful vehicles for understanding and describing the engineering properties of construction materials. With the rapid development of both computational capabilities and theoretical insights into chemical reactions, there have been increasing research activities around the globe and raising demands for computational methods that describe different characteristics of alkali-activated materials. In this Chapter, we summarized the collective efforts performed on modelling and simulation of alkali-activated materials in the past two decades and highlighted the most relevant results and advances in the aspects of atomistic simulation, thermodynamic modelling, kinetics modelling, microstructure simulation, and multi-scale modelling. It can be concluded that pioneering work on modelling and simulation of alkali-activated materials has been conducted with fruitful results. However, there are still deficiency gaps and challenges in modelling and simulation of alkali-activated materials, especially in comparison with PC-based materials.

Keywords Alkali-activated materials · Atomistic simulation · Thermodynamics · Kinetics · Multi-scale modelling

Y. Zuo (✉)
School of Civil and Hydraulic Engineering, Huazhong University of Science and Technology, Wuhan, China
e-mail: zuoyibing@hust.edu.cn

L. Göbel
Chair of Mechanics of Materials, Bauhaus-Universität Weimar, Weimar, Germany

J. Yliniemi
Fibre and Particle Engineering Research Unit, Faculty of Technology, University of Oulu, Oulu, Finland

J. L. Provis
PSI Center for Nuclear Engineering and Sciences, Paul Scherrer Institut (PSI), Villigen, Switzerland

G. Ye
Section of Materials and Environment, Faculty of Civil Engineering and Geosciences, Delft University of Technology, Delft, The Netherlands

© RILEM 2026

G. Ye and F. Dehn (eds.), *Mechanical Properties of Alkali-Activated Materials*, RILEM State-of-the-Art Reports 46, https://doi.org/10.1007/978-3-032-07116-3_5

1 Introduction

With the rapid development of both computational capabilities and theoretical insights into chemical reaction processes, numerical models have been well developed and widely used in the studies of Portland cement (PC) based materials, which provides us with an important numerical study route in addition to the experimental one [1, 2]. In recent years, the accelerating interest in alkali activated-materials (AAMs), as highlighted in earlier chapters of this State of the Art Report, has generated increasing research activities around the globe, and raised the demand for numerical models that describe different characteristics of AAMs. This Chapter presents the state-of-art in modelling and simulation of AAMs, and highlights the most relevant results in terms of the following five parts, divided by length scale from the nanoscale to the macroscale:

- Atomistic simulation of C–(N–)A–S–H and N–A–S–H gels
- Thermodynamic modelling of AAMs
- Kinetic modeling of AAMs
- Simulation of the microstructure formation of AAMs
- Multiscale micromechanical modelling of AAMs.

With this review, a reference for evaluating the recent advances in modelling and simulation approaches is provided. It is concluded by outlining further perspectives for future computer-based investigations and developments regarding AAMs.

2 Atomistic Simulation of C–(N–)A–S–H and N–A–S–H Gels

Within the last decade, several models reproducing the molecular mechanisms occurring in AAM have been developed. The main focus of such models is to describe the chemistry and nanostructure of the key strength-giving phases in AAMs: the tobermorite-like C–(N–)A–S–H gels in high-Ca binders, and the zeolite-like N–A–S–H gels in low-Ca binders. Several atomistic modelling approaches have been developed, unravelling the chemical structures of AAM and the factors influencing them [3–6]. White and colleagues have particularly focused on the aqueous and pre-nucleation aspects of alkali-activation via atomistic approaches [7, 8], providing essential information that can be used to advance the understanding of the gels themselves.

Considering first the high-Ca end of the AAMs spectrum, Puertas et al. [9] applied atomistic simulation approaches using a force field-based method to simulate the structural formation of C–A–S–H gel during the alkaline activation of slag. In their model, a tobermorite-like structure for the C–A–S–H gel was assumed. Those authors found that the nature of the alkaline activating solution entails different mechanical states of the gel. Myers et al. [10] described the C–(N)–A–S–H gel as a mixture

of cross-linked and non-cross-linked tobermorite-based structures, defining the so-called cross-linked tobermorite model, and these structural descriptions have opened further opportunities for detailed analysis and simulation of complex chain-structured silicates that are relevant to high-Ca AAM binders [11].

Lolli et al. [12] studied the impact of disorder on the structure and mechanics of AAM by introducing nanoscale interfacial zones between crystalline and amorphous nanodomains. The behavior of N–A–S–H gels at high temperature has been described [4], and the essential roles of water and Si/Al ratio in defining material properties have also been investigated in detail [13].

It should be noted that it is not straightforward to define and develop an accurate structural simulation for N–A–S–H gels, because their disorder means that rather large simulation cells need to be used, but simply simulating a disordered box of alkali-aluminosilicate units tends to yield a glassy structure rather than accurately representing the partial local ordering and zeolite-like structural motifs that can be identified experimentally. This error is particularly difficult to avoid when simulations are conducted at elevated temperatures to accelerate the rate of cross-linking in the simulation; a not-uncommonly used methodology is to run a high-temperature and/or anhydrous structural simulation and then later add water to generate a "hydrous gel" structure. Unfortunately, the results published to date from this approach tend to lack the nanostructural ordering of near-ambient temperature synthesized AAM gels. This is a similar issue to those which have been discussed in the past regarding the degree of disorder in simulated C–S–H structures [14], and further highlights the need for additional technique development and very careful interpretation of simulation results when discussing such complex and partially-disordered hydrous silicate structures. In this regard, the work of Lolli et al. [12] focused on identifying the causes and nature of disorder in N–A–S–H models can be seen to bring significant value.

3 Thermodynamic Modelling of AAMs

Thermodynamics is of great significance for understanding chemical reactions [15]. The chemical reactions in AAMs, similar to any other chemical system, follow the laws of thermodynamics, although kinetic factors are clearly important. Since the relatively close approach to (stable or metastable) equilibrium has been observed through many stages of the reaction processes, thermodynamic modelling can be a valuable tool in the analysis of AAMs.

Figure 1 shows a schematic illustration of the application of thermodynamic principles to the discussion of reaction processes in AAMs. When aluminosilicate precursors are brought into contact with an alkaline activator, their constituents start to dissolve because the aqueous phase is highly undersaturated with respect to the solid phases present, leading to an increase of the concentrations of aqueous ions in solution as shown by the red curve (*kinetics*). When the concentrations of the

aqueous ions increase to a certain level, such that the solution is saturated or supersaturated with respect to specified solid reaction products, these aqueous ions are thermodynamically favored to precipitate and form those solid reaction products. According to the Ostwald stage rule, the initially-formed solid phases are likely to be less stable than the final thermodynamically preferred products, and so there is the possibility that these will either evolve or re-form toward more stable structures. Consequently, the concentrations of these aqueous ions start to decrease. Afterwards, two kinds of thermodynamic interactions are present in the system. One thermodynamic interaction is between the precursors and the solution, continuously releasing elements into solution. The other one is between the dissolved species in the solution which undergo nucleation-growth processes involving the surfaces of the solid reaction products, leading to growth of the solid reaction products. Overall, the system of solid phases in equilibrium with an aqueous solution will progressively evolve toward a state that minimizes its Gibbs free energy, subject to kinetic constraints that may, for example, render the dissolution of any residual precursor particles very slow at later age because their surfaces are blocked by dense rims of reaction products. In this process, the precursors are gradually transferred into solid reaction products.

Thermodynamic modelling of AAMs is usually performed by specifying a certain reaction degree of the precursors (i.e. describing kinetic effects a priori or by passing information from a separate kinetic model), in which the equilibrium between the solution and the solid reaction products is assumed. The thermodynamic database used to calculate which phases will form (e.g. enthalpy, entropy and solubility products etc.) of all the solids, aqueous and gaseous species is the key underpinning platform for this type of research. With the thermodynamic database, the thermodynamic modelling of chemical reactions can be carried out by using software tools. The quality of the thermodynamic modelling results is directly dependent on the quality and completeness of the thermodynamic database. In the latest release of the thermodynamic database, referred to as Cemdata18 [16], the reaction products that are uniquely identified in high-Ca AAMs (e.g. alkali-activated slag) have been incorporated, enabling the use of this database for the thermodynamic modelling of high-Ca alkali-activated materials. N–A–S–H phases are not yet fully described in the available databases and so can either be added into simulations directly by

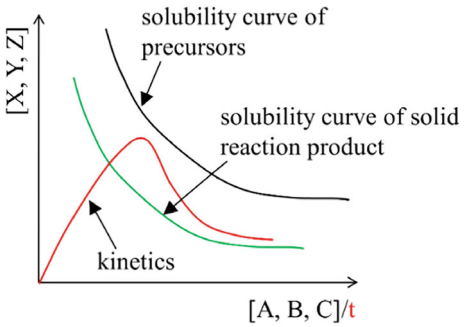


Fig. 1 An illustration of the application of thermodynamic principles to the reaction of AAMs. In the graph, [X, Y, Z] and [A, B, C] represent the concentrations of aqueous ions X, Y, Z and A, B, C, respectively, and t represents time

researchers based on an increasing volume of published solubility data, e.g. [17, 18], or represented by proxy as zeolitic phases (which have similar nanostructure and energetics/solubility).

3.1 Thermodynamic Modelling Approach

Thermodynamic calculations of cement solubility and precipitation processes are commonly conducted using two distinct, but complementary, approaches. In software tools such as GEM-Selektor V3 (http://gems.web.psi.ch/) [19, 20], a system of equations describing the Gibbs free energy of the reaction system is established, and then the Gibbs energy is minimized through a numerical solver kernel to provide a prediction of the phases and aqueous composition present at equilibrium; thermodynamically, an equilibrium state is defined as having the lowest possible Gibbs free energy. Conversely, packages such as PHREEQC [21] rely on a law-of-mass-action based solver to establish and solve a matrix of solubility equilibrium expressions, and the aqueous phase composition is adjusted through dissolution/precipitation processes until all solubility equilibrium relationships are satisfied. Both approaches have their respective advantages and disadvantages in numerical and practical terms, but in principle should be able to give similarly correct outcomes in simulating cementitious and AAM systems if a high quality database (such as Cemdata18, which is available in both GEM-Selektor and PHREEQC formats) and a sufficiently rigorous aqueous activity coefficient model is used.

For the aqueous activity coefficient model, various relationships based on extension of the Debye-Huckel equation are often used to calculate the ion activity coefficients. Equation (1) gives one such model, the Truesdell-Jones formulation, which is often used in GEM-Selektor models for Portland cement hydration [22]:

$$Log_{10}\gamma_j = \frac{-A_\gamma z_j^2 \sqrt{I}}{1 + \dot{a}B_\gamma \sqrt{I}} + b_\gamma I + log_{10}\frac{x_{jw}}{X_w} \tag{1}$$

where γ_j and z_j are the activity coefficient and charge of the aqueous species j, respectively. A_γ and B_γ are electrostatic parameters, I is the ionic strength of the aqueous electrolyte phase, x_{jw} is the molar quantity of water, X_w is the total molar amount of the aqueous phase, and $\dot{a}$ and b_γ are the average ion size and the parameter for common short-range interactions of the dominant charged species in the aqueous environment.

Equation (1) is believed to be valid up to ionic strengths of around 1 mol/kg H_2O [22]; this is sufficient to describe Portland cement hydration, but may be a limitation when investigating the early stages of reaction of AAMs, during which time the ionic strength may be significantly higher than this. Some work on AAM reaction simulation has therefore been focused on applying more advanced models [23], such

as the Pitzer model (which is intended to be applicable up to ~6 mol/kg H_2O) [24], but this is a topic that requires further development.

3.2 *Thermodynamic Database for Thermodynamic Modelling of AAMs*

The thermodynamic database used in modelling AAMs is usually established based on the ones for cement-based materials, supplemented by introducing the solid phases that are uniquely identified as reaction products in AAMs. Any of these phases can be included in the thermodynamic database, once their thermodynamic data are defined.

In experimental characterization of alkali-activated slag based materials, C–(N–)A–S–H gel and Mg–Al layered double hydroxide (LDH) phases are identified as the key reaction products. Myers et al. proposed ideal solid solution models called CNASH_ss and MgAl–OH–LDH_ss, to describe C–(N–)A–S–H gel and Mg–Al LDH phases, respectively, in thermodynamic modelling of AAMs [25, 26]. The CNASH_ss model contains eight end-members denoted as 5CA, INFCA, 5CNA, INFCNA, INFCN, T2C, T5C and TobH (Table 1). Among these eight end-members, 5CA and INFCA are two C–A–S–H end-members, 5CNA and INFCNA are two C–N–A–S–H end-members, INFCN is a C–N–S–H end-member and, T2C, T5C and TobH are three C–S–H end-members. The MgAl–OH–LDH_ss model consists of three end-members, i.e. $Mg_4Al_2(OH)_{14}(H_2O)_3$, $Mg_6Al_2(OH)_{18}(H_2O)_3$ and $Mg_8Al_2(OH)_{22}(H_2O)_3$, respectively. The dissociation reactions and solubility products of those solid phases are tabulated in Table 1 and their thermodynamic properties (data) were provided in [25, 26]. The CASH+ model [27] has also been extended to describe C–(N–)A–S–H chemistry, as well as other alkali and alkali-earth cations that can substitute into the interlayer of C–A–S–H chains, and provides a rigorous sublattice-based structural description for further model developments in future.

N–A–S–H gels can form in parallel with these products in some activated slag or blended AAM binders [28], and as noted above, these can either be described by analogy to zeolites, or modeled directly by using the growing body of solubility data available for them. Other reaction products, such as calcium carbo-/sulfo-aluminate hydrates, hydrogarnets, and strätlingite, already exist in the thermodynamic database that is used for thermodynamic modeling of PC-based materials. It is of interest to note that thermodynamic modelling of alkali-activated slag binders often results in the prediction of formation of a large quantity of strätlingite, which is not always in agreement with experimental results; this requires further investigation and potential refinement of the database, in parallel with more detailed experimental characterization of the reaction products.

In alkali-activated fly ash (or metakaolin) based materials with low or no calcium content in the precursors, N–A–S–H gel is the primary, and often unique, reaction

Table 1 Dissociation reactions and solubility products at 25 °C and 1 bar for the CNASH_ss and MgAl–OH–LDH_ss solid solution models

Solids	Dissociation reactions	$\text{Log}_{10}\ K_s$
CNASH_ss model [25]		
5CA	$(CaO)_{1.25} \cdot (Al_2O_3)_{0.125} \cdot (SiO_2) \cdot (H_2O)_{1.625}$ $\rightarrow 1.25Ca^{2+} + SiO_3^{2-} + 0.25AlO_2^- + 0.25OH^- + 1.5H_2O$	−10.75
INFCA	$(CaO) \cdot (Al_2O_3)_{0.15625} \cdot (SiO_2)_{1.1875} \cdot (H_2O)_{1.65625} + 0.6875OH^-$ $\rightarrow Ca^{2+} + 1.1875SiO_3^{2-} + 0.3125AlO_2^- + 2H_2O$	−8.90
5CNA	$(CaO)_{1.25} \cdot (Na_2O)_{0.25} \cdot (Al_2O_3)_{0.125} \cdot (SiO_2) \cdot (H_2O)_{1.25}$ $\rightarrow 1.25Ca^{2+} + SiO_3^{2-} + 0.25AlO_2^- + 0.5Na^+ + 0.75OH^- + H_2O$	−10.40
INFCNA	$(CaO) \cdot (Na_2O)_{0.34375} \cdot (Al_2O_3)_{0.15625} \cdot (SiO_2)_{1.1875} \cdot (H_2O)_{1.3}$ $\rightarrow Ca^{2+} + 1.1875SiO_3^{2-} + 0.3125AlO_2^- + 0.6875Na^+ + 1.3125H_2O$	−10.00
INFCN	$(CaO) \cdot (Na_2O)_{0.3125} \cdot (SiO_2)_{1.5} \cdot (H_2O)_{1.1875} + 0.375OH^-$ $\rightarrow Ca^{2+} + 1.5SiO_3^{2-} + 0.625Na^+ + 1.375H_2O$	−10.70
T2C	$(CaO)_{1.5} \cdot (SiO_2) \cdot (H_2O)_{2.5} \rightarrow 1.5Ca^{2+} + SiO_3^{2-} + OH^- + 2H_2O$	−11.60
T5C	$(CaO)_{1.25} \cdot (SiO_2)_{1.25} \cdot (H_2O)_{2.5} \rightarrow 1.25Ca^{2+} + 1.25SiO_3^{2-} + 2.5H_2O$	−10.50
TobH	$(CaO) \cdot (SiO_2)_{1.5} \cdot (H_2O)_{2.5} + OH^- \rightarrow Ca^{2+} + 1.5SiO_3^{2-} + 3H_2O$	−7.90
MgAl-OH–LDH_ss model [26]		
M_4AH_{10}	$Mg_4Al_2(OH)_{14}(H_2O)_3 \rightarrow 4Mg^{2+} + 2AlO_2^- + 6OH^- + 7H_2O$	−49.70
M_6AH_{12}	$Mg_6Al_2(OH)_{18}(H_2O)_3 \rightarrow 6Mg^{2+} + 2AlO_2^- + 10OH^- + 7H_2O$	−72.02
M_8AH_{14}	$Mg_8Al_2(OH)_{22}(H_2O)_3 \rightarrow 8Mg^{2+} + 2AlO_2^- + 14OH^- + 7H_2O$	−94.34

product. Other potential reaction products are mostly zeolites. However, the thermodynamic properties of N–A–S–H gel are less known than C–(N–)A–S–H gel. The reason for this is the structural disorder in the highly cross-linked aluminosilicate N–A–S–H gel, whose chemical composition is defined by depending on the precursor composition and alkali activation conditions [29, 30]. Based on the literature studies regarding the structure and chemical composition of N–A–S–H gel, Zuo proposed a solid solution model N(C)ASH_ss to describe the N–A–S–H gel in thermodynamic modelling of low-Ca AAMs [31]. This model also considered the partial uptake of calcium by N–A–S–H gel due to the interactions between the N–A–S–H gel and the aqueous calcium. The N(C)ASH_ss model consists of eight solid solution members as listed in Table 2, and its thermodynamic properties can be found in the Ph.D. thesis of Zuo [31]. In a recent study, Chen et al. synthesized N–A–S–H with various Si/Al ratios and established their thermodynamic database, which provides valuable insights into geopolymer reactions and phase assemblages [32]. The thermodynamic properties of other potential reaction products, such as hydroxysodalite, Na-chabazite and zeolite P, and increasingly also their potassium-containing counterparts, are reported in the literature [33], and in the zeolite20/zeolite21 database which is designed to be used in conjunction with Cemdata18 [34, 35].

Table 2 Chemical reactions and solubility products (Log Ksp) at 25 °C and 1 bar for N–(C–)A–S–H, from [31]

Solids	Dissociation reactions	$Log\ K_{sp}$
NASH_1-1[a]	$(Na_2O)_{0.5} \cdot (Al_2O_3)_{0.5} \cdot (SiO_2)_1 \cdot (H_2O)_1 + 2OH^- \leftrightarrow SiO_3^{2-} + AlO_2^- + Na^+ + 2H_2O$	−6.51
NASH_2-1	$(Na_2O)_{0.5} \cdot (Al_2O_3)_{0.5} \cdot (SiO_2)_2 \cdot (H_2O)_1 + 4OH^- \leftrightarrow 2SiO_3^{2-} + AlO_2^- + Na^+ + 3H_2O$	−8.01
NASH_3-1	$(Na_2O)_{0.5} \cdot (Al_2O_3)_{0.5} \cdot (SiO_2)_3 \cdot (H_2O)_1 + 6OH^- \leftrightarrow 3SiO_3^{2-} + AlO_2^- + Na^+ + 4H_2O$	−9.51
NASH_4-1	$(Na_2O)_{0.5} \cdot (Al_2O_3)_{0.5} \cdot (SiO_2)_4 \cdot (H_2O)_1 + 8OH^- \leftrightarrow 4SiO_3^{2-} + AlO_2^- + Na^+ + 5H_2O$	−11.01
NCASH_1-0.1	$(Na_2O)_{0.05} \cdot (CaO)_{0.45} \cdot (Al_2O_3)_{0.5} \cdot (SiO_2)_1 \cdot (H_2O)_1 + 2OH^- \leftrightarrow SiO_3^{2-} + AlO_2^- + 0.45Ca^{2+} + 0.1Na^+ + 2H_2O$	−8.51
NCASH_2-0.1	$(Na_2O)_{0.05} \cdot (CaO)_{0.45} \cdot (Al_2O_3)_{0.5} \cdot (SiO_2)_2 \cdot (H_2O)_1 + 4OH^- \leftrightarrow 2SiO_3^{2-} + AlO_2^- + 0.45Ca^{2+} + 0.1Na^+ + 3H_2O$	−10.01
NCASH_3-0.1	$(Na_2O)_{0.05} \cdot (CaO)_{0.45} \cdot (Al_2O_3)_{0.5} \cdot (SiO_2)_3 \cdot (H_2O)_1 + 6OH^- \leftrightarrow 3SiO_3^{2-} + AlO_2^- + 0.45Ca^{2+} + 0.1Na^+ + 4H_2O$	−11.51
NCASH_4-0.1	$(Na_2O)_{0.05} \cdot (CaO)_{0.45} \cdot (Al_2O_3)_{0.5} \cdot (SiO_2)_4 \cdot (H_2O)_1 + 8OH^- \leftrightarrow 4SiO_3^{2-} + AlO_2^- + 0.45Ca^{2+} + 0.1Na^+ + 5H_2O$	−13.01

[a] The first and second number after N(C)ASH represent the molar ratio of Si/Al and Na/Al in the solid solution member, respectively

In addition to low- and high-Ca type AAMs, high-Fe AAMs are gaining increasing attention in the scientific literature [36]. In comparison to other main cementitious elements, such as Ca, Si and Al, the modelling of Fe uptake is more challenging because the reduction-oxidation potential of the system affects the aqueous speciation of Fe and the precipitation of Fe-containing phases. While Fe-containing hydrates, such as Fe–Al-hydrogarnets, are included in the CEMDATA18 database for PC-based materials, appropriate thermodynamic data are missing for high-Fe AAMs, and it has also been identified that it is possible that some of the literature data for entropy of formation in the Fe-containing hydrate phase could benefit from reassessment [37].

3.3 Application of Thermodynamic Modelling to AAMs

Thermodynamic modelling has been commonly applied in AAMs, allowing for the calculation of stable phase assemblages and aqueous phase compositions at the final state of the completed reaction. On the basis of the thermodynamic database that is relatively well developed for alkali-activated slag-based materials, many studies have been carried out. Myers et al. conducted a series of thermodynamic modelling studies

on the phase diagrams of alkali-activated slag cements under various alkali activation conditions and with different chemical compositions of slag [25, 26, 28]. Figure 2 shows an example of the simulated solid phase evolution of a sodium silicate activated slag paste as a function of the percentage of the slag that has reacted. The solid phase predictions were in general well aligned with the experimentally-determined solid phase assemblage, other than the uncertainty mentioned above regarding strätlingite. Other researchers have also performed thermodynamic modelling of alkali-activated slag cement, focusing on different aspects. For instance, Ye and Radlińska used thermodynamic modelling to investigate the chemical shrinkage of alkali-activated slag [38], and Zuo et al. conducted a comprehensive study to evaluate the thermodynamic modelling results via experimental data [39].

Recently, thermodynamic modelling has been also used to investigate the interactions between alkali-activated slag cement and potentially aggressive ingredients. Ke et al. proposed thermodynamic modelling to describe carbonate-intercalated hydrotalcite, and used this information to study the phase evolution in alkali-activated slag cements exposed to carbon dioxide [40]. The model was able to provide detailed prediction of the influence of carbonation on the chemical structure of alkali-activated slag binders, as the C–(N–)A–S–H is progressively replaced by $CaCO_3$ and a sodium-rich aluminosilicate gel. Park et al. used a similar methodology to focus on the effects of different activators in carbonation of slag-based binders [41]. Zuo established thermodynamic models to describe chloride and sulfate intercalated hydrotalcites and investigated the phase diagrams in alkali-activated slag cements upon attacks by chloride salt [42] and sulfate salt [43], and Mundra et al. [44] used thermodynamic

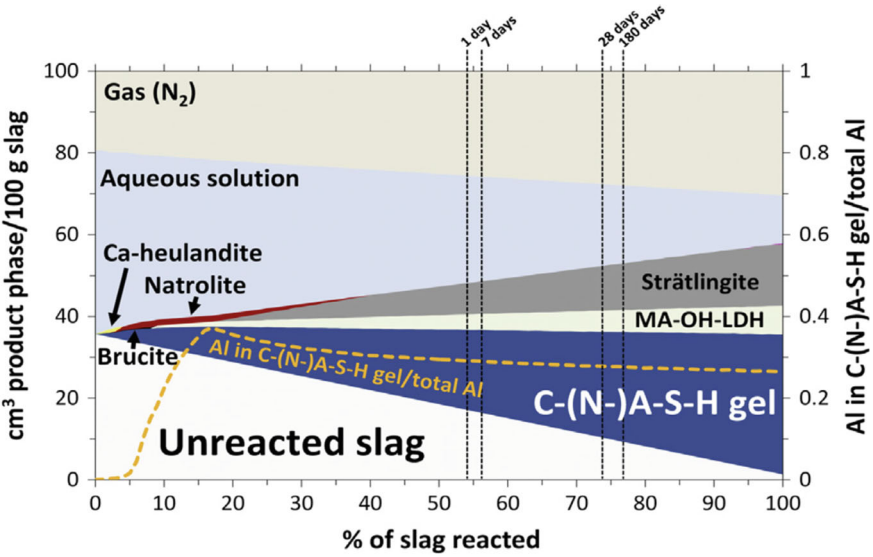


Fig. 2 Simulated phase evolution of a sodium silicate activated slag cement by thermodynamic modelling. Reproduced with permission from Ref. [26]. Copyright 2015, Elsevier BV, Amsterdam

modelling to establish a lookup table-style database of binder mineralogy and pore fluid compositions to underpin a simulation of chloride transport into, and effects on, alkali-activated slag binders.

The extensive thermodynamic studies carried out on alkali-activated slag reveal that the prediction results of the thermodynamic modelling are in good agreement with experimental data retrieved from our own experiments or obtained from the literature. This demonstrates that thermodynamic modelling is a valuable tool for studying and predicting durability performance of alkali-activated slag cements.

Conversely, the thermodynamic modelling of low-Ca-alkali-activated materials and its blends with high-Ca-alkali-activated materials is rarely reported in the literature. This is mainly due to lower availability of thermodynamic data for AAM with low-Ca contents. Zuo conducted thermodynamic modelling of alkali-activated fly ash and its blends with slag [31]. The modelling results show a satisfactory agreement with experimental data in terms of N–A–S–H gel composition and pore solution chemistry, although more experimental data are needed for improving the quality of the thermodynamic data of the N–A–S–H gel. Recently, Chen et al. used the N(C)ASH_ss model to simulate the phase assemblages of alkali-activated municipal solid waste incineration (MSWI) bottom ash pastes, and concluded that the modeling results can be used as references for the mix design of MSWI bottom ash based AAM [45]. It is worth noting that the N(C)ASH_ss model for describing the N–A–S–H gel was semi-empirically established based on experimental observations. Although Chen et al. established the thermodynamic database for N–A–S–H gels [32], whether this database is suitable for conducting thermodynamic modelling of the low-calcium AAMs needs more experimental data to validate.

4 Kinetic Modelling of AAMs

Understanding the reaction kinetics of AAMs is of great significance since it governs the microstructure development and thus microstructure-related properties, including mechanical properties and durability performance. Isothermal calorimetry, as a well-accepted experimental technique for studying the reaction kinetics of PC-based materials, has also been widely used to investigate the reaction kinetics of AAMs, such as the effects of temperature [46, 47] and the type and amount of the alkaline activator [48, 49]. This means that calorimetric data are an obvious starting point to use in developing a kinetic model; these and other pieces of information have formed the basis of several empirical models that have been published. Compared to experimental characterization of reaction processes, the kinetic modelling of AAMs is relatively less intensively studied.

4.1 Application of Simplified Kinetic Models to AAMs

The overall kinetics modelling is usually carried out by using existing models that have initially been developed for PC-based materials, to describe the reaction kinetics of AAMs via fitting the heat release curves experimentally measured by isothermal calorimetry [50, 51], or extent of reaction measurements by other techniques [52, 53]. Table 3 lists some of the simplified models that have been applied in modelling the reaction kinetics of AAMs.

The shrinking core (sometimes called "contracting volume") model [54] can be used to describe the reaction kinetics if the rate of dissolution (or another form of reaction) of a particle is determined by a chemical reaction [55]. However, the formation of reaction products around precursor grains may also make diffusion as the dominant rate controlling process during the reaction process [56]. Using a steady-state solution of Fick's first law, the Ginstling-Brounshtein model can be developed for a spherical particle [57], and correctly accounting for the particle surface curvature [58]. To incorporate the possibility of the rate-controlling process switching between these options as the material microstructure evolves, Parrot and Killoh [59] developed a widely-used model for cement hydration which includes description of changes in rate-controlling step as the diffusional effects become progressively more important at different stages of that chemical reaction process. Their description of diffusion control was based on the incorrect Jander expression (see below), but the model nonetheless continues to be extensively used.

A very simplified first-order reaction model, in which the rate of reaction is proportional to the remaining quantity of one reagent, integrates to give a simple exponential form that has been used to describe calorimetric and other kinetic data sets for AAMs.

There are also several models indicated in Table 3 as lacking a sound physical basis, but which are nonetheless applied regularly in the cements and AAMs literature. The use of such models must be discouraged, but they are included here for completeness.

As an attempt to take diffusional processes into account, Jander's model was proposed based on an attempted solution to Fick's parabolic law, originally for diffusion-controlled reactions in solid state sintering. However, it should be noted that Jander's model was based on a fundamentally flawed mathematical derivation, in which the particle surface curvature was neglected when substituting the expression for $\alpha(t)$ defined in spherical coordinates into a diffusion control equation defined in Cartesian coordinates [58]. For this reason, Jander's model is strictly not correct, particularly at higher reaction extents, and thus not suitable to describe and model the reaction kinetics of AAMs. In order to model consecutive and overlapping reaction processes, researchers have also introduced a reaction grade or exponent N into Jander's model (sometimes termed the "modified Jander's model") and applied it to model the reaction kinetics of AAMs. There is no physical basis for the application of this exponent—nor the application of a similar empirical modification to the Ginstling-Brounshtein equation—and so these models are also noted in Table 3 as

Table 3 Simplified kinetic models that are applied to analysis of AAM reaction processes. Entries shaded in gray are the models which are used despite lacking an explicit mathematical derivation from physical principles

Model	Formula	Notes
Shrinking core model with chemical reaction control	$1-\left(1-\alpha(t)\right)^{1/3}=K_1 t$ $K_1=\frac{k_1}{r_0}$	$\alpha(t)$: degree of reaction at time t; k_1: rate constant; r_0: initial radius of a sphere;
Ginstling-Brounshtein model (shrinking core with diffusion control)	$1-\frac{2}{3}\alpha(t)-\left(1-\alpha(t)\right)^{2/3}=kt$ $k=\frac{D\cdot C_2\cdot\mu}{\rho\cdot n}$	D: diffusion coefficient; C_2: concentration of reactant; μ: molecular weight;
First-order (exponential rate control)	$\alpha(t)=1-e^{-k_r t}$	ρ: density; n: stoichiometric coefficient; k_r: first-order rate constant;
Jander's model	$\left[1-\left(1-\alpha(t)\right)^{1/3}\right]^2=K_2 t$ $K_2=\frac{k_2}{R^2}$	k_2: diffusion constant; R: initial radius of a reacting sphere
Modified Jander's model	$\left[1-\left(1-\alpha(t)\right)^{1/3}\right]^N=K_2 t$ $K_2=\frac{k_2}{R^2}$	N: reaction grade;
Modified Ginstling-Brounshtein model	$\left[1-\frac{2}{3}\alpha(t)-\left(1-\alpha(t)\right)^{2/3}\right]^N=kt$ $k=\frac{D\cdot C_2\cdot\mu}{\rho\cdot n}$	

being disfavoured. It is often claimed that the value of N represents the rate controlling mechanisms. For example, it is stated that when $N < 1$, reaction occurs through the nucleation kinetic control; when N is close to 1, reaction occurs through the phase-boundary kinetic control; when $N > 1$, reaction occurs through the diffusion kinetic control. However, because the underlying equation being modified by this exponent is derived explicitly from the physics of diffusion control in a shrinking-core particle,

there is not any theoretical basis for the identification of these values of N taking any mechanistic significance, and these interpretations should be discarded. Similar arguments may also be applied to the empirical fitting of exponents in the so-called JMAK or Avrami-Erofe'ev model for application to AAM reactions; these models have a physically-based derivation that describes a particular geometry and rate control mechanism in metallurgical processes, and because the physical processes described are not correct in describing alkali-activation kinetics, it is difficult to see how the interpretation of parameter values could somehow remain valid.

The kinetic models as tabulated in Table 3, despite satisfactorily describing the reaction kinetics, are in general unable to produce a priori prediction of reaction kinetics of AAMs, particularly considering the wide diversity of precursors, alkali activators and their massive combinatorial spaces. This is because they are based partly on theoretically-derived kinetic mechanisms and partly on assumptions. In recent years, machine learning and its use in predicting properties of cement-based materials has gained a great momentum. Reaction kinetics, as one of these properties, has been also successfully and priorly predicted via machine learning models for PC-based materials [60, 61]. This suggests that future work pertaining to overall kinetic modelling of AAMs should consider the use of machine learning.

4.2 Chemical Mechanism-Based Modelling of the Geopolymerization Process

In addition to the overall kinetic modelling of AAMs, many researchers focus on the kinetic modelling of the geopolymerization process in low-Ca-alkali-activated materials, such as alkali-activated metakaolin and fly ash. Based on an aluminosilicate weathering model that had originally been proposed to analyze the dissolution and reprecipitation steps with an overall reaction process [62], Provis et al. developed a reaction kinetic model, highlighting certain factors that determined the setting rate of alkali-activated metakaolin, taking into account varying SiO_2/Al_2O_3 ratios [53, 63]. Figure 3 shows the scheme of the modified reaction kinetic model, based on which, the kinetic expressions to describe these reactions were established and thus the reaction processes numerically simulated. Although it probably still needs to be developed further based on a broader set of experimental data, the results showed that this modified reaction kinetic model was able to provide a plausible description of the reaction process of alkali-activated metakaolin or fly ash. With this kinetic model, Zhang et al. estimated the reaction enthalpies and thus quantified the reaction extent of alkali-activated metakaolin [50, 64].

White et al. [3] also simulated the reaction processes in alkali-activation of metakaolin by developing a multi-scale approach whereby atomistic descriptions of individual chemical reaction steps (i.e. bond formation between individual small species) were then coarse-grained into a mesoscale description of structure formation on the nanometer length scale. This approach was then later extended to broader

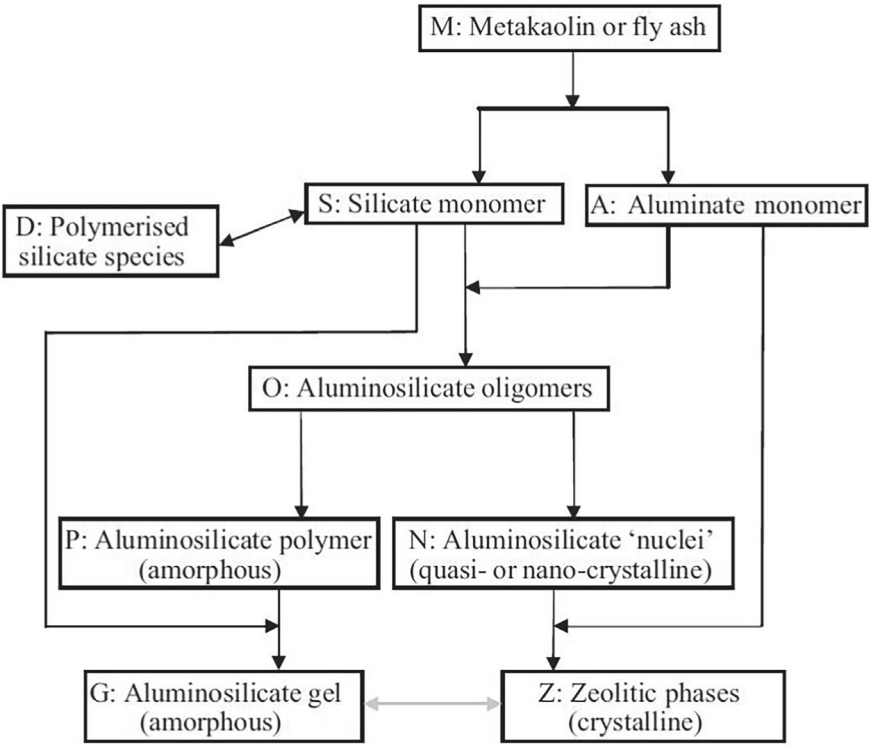


Fig. 3 Scheme of the modified reaction kinetic model of alkali-activated metakaolin or fly ash. Reproduced with permission from Ref. [63]. Copyright 2007, Elsevier BV, Amsterdam

compositional and morphological ranges [65], and also applied to predict pore structure formation and evolution in low-calcium AAMs [66].

In another study by Valentini, the geopolymerization kinetics of metakaolin based geopolymer was kinetically simulated by the HydratiCA model; this work provided further detailed insight into the various reaction steps including nucleation and growth effects, and demonstrated that the reaction pathways greatly depends on the composition and concentration of alkali activators [67].

5 Simulation of the Microstructure Formation of AAMs

Similar to PC-based materials, AAMs are also porous materials. The microstructure of these porous materials dictates the development of their mechanical and durability properties. In the literature there are many numerical models available to simulate the micro- and pore structure development of PC-based materials, such as CEMHYD3D [68], μic model [69] and HYMOSTRUC3D [70]. However, those models are not

immediately capable of studying the microstructural development of AAMs since the reaction process and microstructure formation of AAMs are intrinsically different from those of PC-based materials. For this reason, the microstructure-related properties of AAMs, such as tensile strength, permeability and diffusivity of chloride etc., are less studied numerically as compared to those of PC-based materials.

The microstructure development of AAMs is accompanied by a series of processes. These include the initial particle parking structure of precursor grains in alkaline solution, dissolution of precursor grains, diffusion/transport of ions, chemical reactions of ions and nucleation and growth of reaction products. The processes are inter-dependent and dictate the microstructure development of AAMs. By strictly following the simulations of these processes, Zuo and Ye proposed a novel framework (GeoMicro3D) for developing numerical models to simulate the microstructure formation of AAMs [71]. Figure 4 illustrates the scheme of the numerical framework. The first module aims to generate the initial particle parking structure of precursor grains in an alkaline activator solution using real-shape particles. The second module is aimed at the simulation of the dissolution process of precursor grains in alkaline activator solutions. The third module aims to simulate the transport of aqueous ions in the simulation system by using the lattice Boltzmann method. In the fourth module, the reactions of aqueous ions are simulated and quantified by means of thermodynamic modelling. In the last module, a nucleation probability theory is used to consider the nucleation and growth of reaction products in the simulation system. In such a way, the reaction process and microstructure development of AAMs can be simulated numerically.

Later, Zuo et al. implemented this novel numerical framework to simulate the reaction process and microstructure development of alkali-activated slag cement paste [31, 72]. The simulation results were discussed and compared with relevant experimental data, such as reaction degree of slag and pore solution composition, demonstrating a good agreement in the comparisons. Figure 5 shows four stages of the simulated microstructures of alkali-activated slag cement paste at time instants of 0, 3 h, 1 day and 7 days, respectively. The colors of blue and gray represent liquid and slag, respectively. The yellow color represents the reaction front cells within which slag may dissolve and reaction products may also precipitate. The colors of red and green represent the cells that are partially and completely filled with reaction products, respectively. It can be readily seen from these pictures that reaction products grow and thus microstructure develops. More comparisons and discussion, such as reaction kinetics, pore solution chemistry and volume evolution of phases etc., can be referred to the literature studies [31, 72].

GeoMicro3D is a robust model in studying the reaction process and microstructural development of AAMs. Table 4 presents the functionalities of GeoMicro3D. With GeoMicro3D at hand, it is possible to perform numerical studies on the microstructure-related properties such as tensile strength, permeability and diffusivity of chloride, among others. Very recently, a numerical model was proposed to study chloride transport in AAMs based on GeoMicro3D and implemented to simulate chloride transport in alkali-activated slag cement paste [73]. The effective diffusivity in paste was simulated between 6×10^{-13} and 5×10^{-12} m^2/s, smaller than

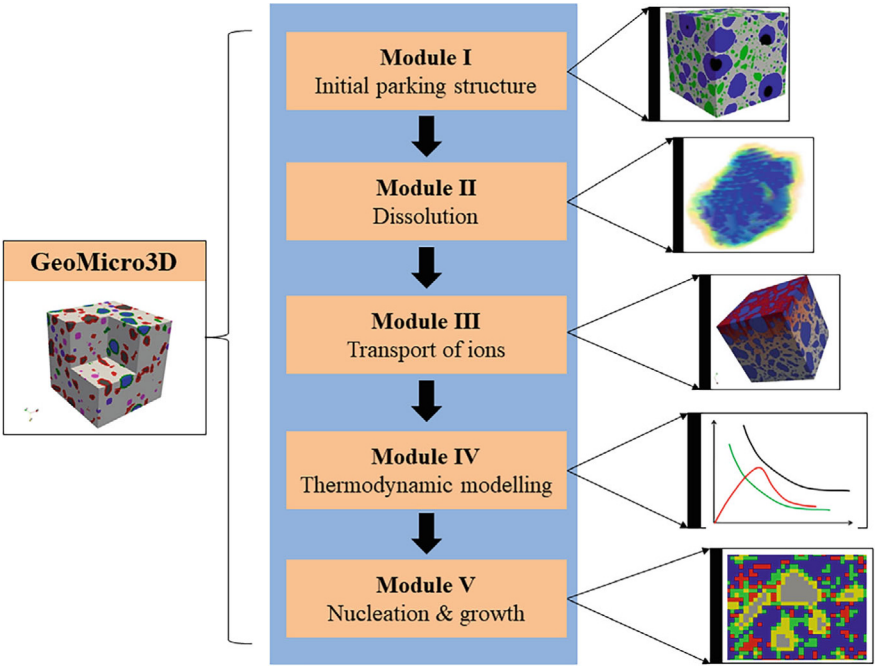


Fig. 4 Modelling scheme of the framework [71]

that (10^{-12} and 10^{-11} m^2/s) in concrete [74, 75]. This simulation result is reasonable since the concrete usually has high porosity due to interfacial transitional zone.

6 Multiscale Micromechanical Modelling of AAMs

The differing chemical compositions of the two types of gels formed in AAMs inherently entails differences in their structures. C–A–S–H gels commonly exhibit a tobermorite-like structure [10, 76], while N–A–S–H gels are characterized by a disordered structure and a network resembling the short-range structure of nanocrystalline zeolites [29, 77, 78]. Reliable modeling strategies for AAM should therefore link the binder chemistry and the resulting nano- or microstructural characteristics with the mechanical behavior at the macroscopic scale.

An accepted modelling approach aiming to connect several scales of observation of a material rests on continuum micromechanical homogenization theory. Such models have broadly been applied to estimate the mechanical properties of cementitious materials, such as the elastic stiffness (see e.g. [79–81]), strength (see e.g. [82, 83]), autogenous shrinkage (see e.g. [84]) as well as creep properties (see e.g. [85, 86]). Some authors have also applied these semi-analytical micromechanics-based

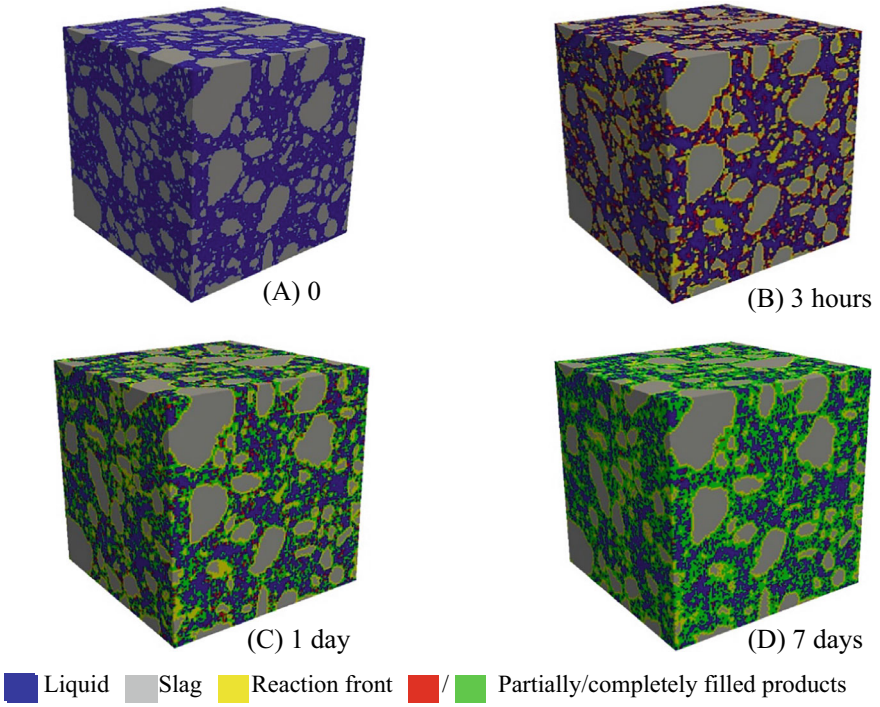


Fig. 5 Simulated 3D microstructures of sample BFS_N4S0 at 0, 3 h, 1 day and 7 days. The size of the cubic simulation cell is 125 × 125 × 125 μm. The digitization resolution is 1 × 1 × 1 μm per voxel [31]

Table 4 Functionalities of GeoMicro3D

Functionality	GeoMicro3D
Available systems	Mono system: AAS, AAFA Binary system: AA BFS/FA
Degree of reaction of precursor	Available
Pore solution chemistry	Available
Microstructure formation	Available
Volume evolution of solid phases	Available
Distribution of reaction products	Available
Distribution of ions	Available
Element composition of each cell	Available
Evolution of capillary porosity	Available
Evolution of gel porosity	Available
Parallelization of codes	Yes

models to modern generations of building materials, i.e. to blended or polymer-modified cementitious mortars and concretes [87–89] and to concretes with recycled aggregates [90, 91].

For AAMs, multiscale modelling also attracts an increasing research attention. Šmilauer et al. [92] developed a micromechanical model using semi-analytical homogenization for the prediction of the elastic stiffness for alkali-activated fly ash and metakaolin. A two-scale micromechanical representation of the materials was established, in which the so-called N–A–S–H level and the paste level were distinguished. The former includes poorly crystallized reaction products, introduced as solid gel particles, and the latter contains unreacted material remnants and the open porosity. The time-dependent stiffening of the N–A–S–H gel could well be captured by increasing the fraction of solid gel particles, which individually differ regarding their packing density and their intrinsic elastic stiffness for fly ash and metakaolin, respectively. The micromechanical estimates are in good agreement with experimentally determined values. Das et al. [93] used two mean-field homogenization methods, namely the Mori-Tanaka scheme and the double inclusion model, in order to predict stiffness properties of activated fly ash pastes. The macroscopic homogenized values for the Young's modulus of the mixture revealed satisfactory results. The Mori-Tanaka approach provides slightly larger values because it does not consider interactions between the different inclusions. The results of the double inclusion method were found to closer capture the experimental stiffness values because it represents the material's heterogeneity more accurately.

A further micromechanical approach for the stiffness homogenization of alkali activated fly ash-slag pastes has been proposed by Fang et al. [94]. The material was represented by three consecutively arranged representative volume elements (RVE), as shown in Fig. 6. At a scale of a few nanometers, solid gel particles are defined. The gel matrix scale comprises the dimensions between 10 nm and 1 μm and included the solid gel particles and gel pores. The paste scale, with a size of a few micrometers, distinguished capillary pores and unhydrated slag and fly ash particles. Throughout the model, all phases are assumed to exhibit a spherical shape. Nanoindentation provided access to the phase volume fractions. Effective elastic, bulk, and shear moduli for varying curing ages were derived. The homogenization results revealed fluctuant values for the elastic and bulk moduli with time, but more or less stable values for the shear modulus. However, the micromechanical analyses need further refinement.

Recently, Jiang et al. [95] illustrated the potential of correlating micromechanical analyses and modeling approaches with the macroscopic mechanical behavior of alkali-activated slag. The authors applied thermodynamic and molecular dynamic modeling to obtain information about the microstructural development. Homogenization theory was also applied by Caron et al. [96] to evaluate elastic stiffness properties of alkali-activated slag concretes. As shown in Fig. 7, a five-step model up to the concrete scale was proposed, in which the following levels are distinguished: Level 0 includes soft and hard reaction products as well as the gel water. Elastic stiffness values for the two matrix types are obtained from nanoindentation experiments. Level 1 additionally introduces water pores into this matrix. Level 2

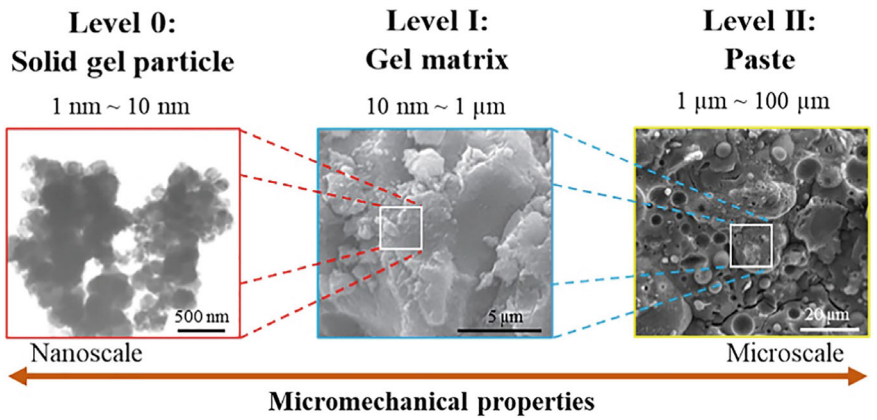


Fig. 6 Schematic illustration of multiscale micromechanical analysis. Reproduced with permission from Ref. [94]. Copyright 2020, Elsevier BV, Amsterdam

considered unreacted slag particles embedded in the homogenized matrix obtained from Level 1. Level 3 corresponds to the mortar scale and additionally includes sand grains with an ITZ, while Level 4 corresponds to the concrete scale with the respective aggregates. By comparing the modeling results with experimental stiffness values derived from ultrasound tests, Caron et al. pointed out the importance of separating the total porosity between the Levels 0 and 1 because otherwise the Young's modulus is underestimated. At the scales of paste and concrete, i.e. for stiffness values at a sample age of 28 days, a model accuracy of 95% was achieved. Further sensitivity analyses were performed to elucidate the importance of further model input parameters. The results indicate that the ITZ at the mortar scale can be neglected in further analyses and that the most influential parameters are the properties related to the soft matrix. The composition of the activating solution also has a large influence on the modeling results, more so than the slag composition.

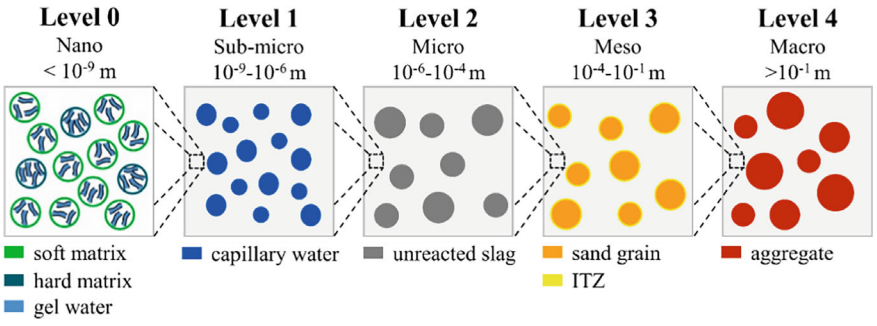


Fig. 7 Schematic representation of five-step model. Reproduced with permission from Ref. [96]. Copyright 2023, Elsevier BV, Amsterdam

7 Conclusion and Perspectives

During the last years, pioneering work on modelling and simulation of AAMs has been conducted with fruitful results. However, compared to the established advanced modelling and simulation techniques developed for the application to PC-based materials, numerical research on AAMs is in its infancy that, however, attracts more and more attention from the research community. Although many models and simulation methods have been originally developed for PC-based materials, these models and methods cannot be directly used for AAMs. The reasons are the intrinsic differences between PC-based materials and AAMs in the aspects of reaction mechanism, reaction products, microstructure formation and pore solution chemistry. In the future, more attention should be directed to the following aspects regarding modelling and simulation of AAMs:

- Atomistic models are usually developed separately to reproduce the molecular mechanisms of C–(N–)A–S–H and N–A–S–H gels for alkali-activated high-Ca and low-Ca systems, respectively. There is a lack of atomistic modelling work devoted to blends of C–(N–)A–S–H and N–A–S–H gels and exploring their interaction mechanisms.
- The thermodynamic database is well developed for AAMs with high-Ca content while it is still incomplete for AAMs with low to no calcium, and for high-Fe phases, which limits the application of thermodynamic modelling to AAMs. Although the N(C)ASH_ss model for describing the N–A–S–H gel was developed, it is desirable to develop a thermodynamic model from the mechanistic point of view via atomistic simulation.
- Due to the wide diversity of precursors, alkali activators and their massive combinatorial spaces, traditional kinetic models are unable to produce a priori prediction of reaction kinetics of AAMs. In this situation, machine learning shows a great potential to predict the reaction kinetics of AAMs.
- Many properties are dependent on the microstructure of AAMs, but there are only a few numerical models available and suitable for simulating the microstructure formation of AAMs as those developed for PC-based materials. GeoMicro3D is developed for the first time to simulate the reaction process and microstructure formation of AAMs, but it still needs further development and verification.
- Currently, only a few researchers have focused on the microstructure-based and multiscale modelling of AAMs, in which analytical homogenization theory was mainly used. However, for predicting the durability of various AAMs that cover e.g. transport of ions or aggressive media, numerical studies should also be established accounting for the spatial structure of AAMs. In this regard, GeoMicro3D could be a prerequisite for such attempts.

References

1. Dolado, J.S., van Breugel, K.: Recent advances in modeling for cementitious materials. Cem. Concr. Res. **41**, 711–726 (2011)
2. Thomas, J.J., Biernacki, J.J., Bullard, J.W., Bishnoi, S., Dolado, J.S., Scherer, G.W., Luttge, A.: Modeling and simulation of cement hydration kinetics and microstructure development. Cem. Concr. Res. **41**, 1257–1278 (2011)
3. White, C.E., Provis, J.L., Proffen, T., van Deventer, J.S.J.: Molecular mechanisms responsible for the structural changes occurring during geopolymerization: multiscale simulation. Aiche J **58**, 2241–2253 (2012)
4. Kupwade-Patil, K., Soto, F., Kunjumon, A., Allouche, E.N., Mainardi, D.S.: Multi-scale modeling and experimental investigations of geopolymeric gels at elevated temperatures. Comput. Struct. **122**, 164–177 (2013)
5. Wan, X., Hou, D., Zhao, T., Wang, L.: Insights on molecular structure and micro-properties of alkali-activated slag materials: a reactive molecular dynamics study. Constr. Build. Mater. **139**, 430–437 (2017)
6. Chitsaz, S., Tarighat, A.: Molecular dynamics simulation of N–A–S–H geopolymer macro molecule model for prediction of its modulus of elasticity. Constr. Build. Mater. **243**, 118176 (2020)
7. Yang, K., White, C.E.: Modeling of aqueous species interaction energies prior to nucleation in cement-based gel systems. Cem. Concr. Res. **139**, 106266 (2021)
8. Gong, K., Yang, K., White, C.E.: Density functional modeling of the binding energies between aluminosilicate oligomers and different metal cations. Front. Mater. **10**, 1089216 (2023)
9. Puertas, F., Palacios, M., Manzano, H., Dolado, J.S., Rico, A., Rodríguez, J.: A model for the C–A–S–H gel formed in alkali-activated slag cements. J. Eur. Ceram. Soc. **31**, 2043–2056 (2011)
10. Myers, R.J., Bernal, S.A., San Nicolas, R., Provis, J.L.: Generalized structural description of calcium–sodium aluminosilicate hydrate gels: the cross-linked substituted tobermorite model. Langmuir **29**, 5294–5306 (2013)
11. Yang, J., Hou, D., Ding, Q.: Structure, dynamics, and mechanical properties of cross-linked calcium aluminosilicate hydrate: a molecular dynamics study. ACS Sustain. Chem. Eng. **6**, 9403–9417 (2018)
12. Lolli, F., Manzano, H., Provis, J.L., Bignozzi, M.C., Masoero, E.: Atomistic simulations of geopolymer models: the impact of disorder on structure and mechanics. ACS Appl. Mater. Interfaces 22809–22820 (2018)
13. Sadat, M.R., Bringuier, S., Asaduzzaman, A., Muralidharan, K., Zhang, L.: A molecular dynamics study of the role of molecular water on the structure and mechanics of amorphous geopolymer binders. J. Chem. Phys. **145**, 134706 (2016)
14. Richardson, I.: The importance of proper crystal-chemical and geometrical reasoning demonstrated using layered single and double hydroxides. Acta Crystallogr. Sect. B **69**, 150–162 (2013)
15. Damidot, D., Lothenbach, B., Herfort, D., Glasser, F.P.: Thermodynamics and cement science. Cem. Concr. Res. **41**, 679–695 (2011)
16. Lothenbach, B., Kulik, D.A., Matschei, T., Balonis, M., Baquerizo, L., Dilnesa, B., Miron, G.D., Myers, R.J.: Cemdata18: a chemical thermodynamic database for hydrated Portland cements and alkali-activated materials. Cem. Concr. Res. **115**, 472–506 (2019)
17. Gomez-Zamorano, L., Balonis, M., Erdemli, B., Neithalath, N., Sant, G.: C–(N)–S–H and N-A–S–H gels: Compositions and solubility data at 25 and 50 °C. J. Am. Ceram. Soc. **100**, 2700–2711 (2017)
18. Walkley, B., Ke, X., Hussein, O., Provis, J.L.: Thermodynamic properties of sodium aluminosilicate hydrate (N–A–S–H). Dalton Trans. **50**, 13968–13984 (2021)
19. Kulik, D.A., Wagner, T., Dmytrieva, S.V., Kosakowski, G., Hingerl, F.F., Chudnenko, K.V., Berner, U.R.: GEM-Selektor geochemical modeling package: revised algorithm and GEMS3K numerical kernel for coupled simulation codes. Comput. Geosci. **17**, 1–24 (2013)

20. Wagner, T., Kulik, D.A., Hingerl, F.F., Dmytrieva, S.V.: GEM-Selektor geochemical modeling package: TSolMod library and data interface for multicomponent phase models. Can. Mineral. **50**, 1173–1195 (2012)
21. Parkhurst, D.L., Appelo, C.: Description of input and examples for PHREEQC version 3—A computer program for speciation, batch-reaction, one-dimensional transport, and inverse geochemical calculations. In: US Geological Survey Techniques and Methods, Book 6, Chap. A43: 497 (2013)
22. Lothenbach, B.: Thermodynamic equilibrium calculations in cementitious systems. Mater. Struct. **43**, 1413–1433 (2010)
23. Caron, R., Patel, R.A., Miron, G.D., Le Galliard, C., Lothenbach, B., Dehn, F.: Microstructure development of slag activated with sodium silicate solution: experimental characterization and thermodynamic modeling. J. Build. Eng. **71**, 106398 (2023)
24. Pitzer, K.S.: A thermodynamic model for aqueous solutions of liquid-like density. Rev. Mineral. Geochem. **17**, 97–142 (1987)
25. Myers, R.J., Bernal, S.A., Provis, J.L.: A thermodynamic model for C–(N–)A–S–H gel: CNASH_ss. Derivation and validation. Cem. Concr. Res. **66**, 27–47 (2014)
26. Myers, R.J., Lothenbach, B., Bernal, S.A., Provis, J.L.: Thermodynamic modelling of alkali-activated slag cements. Appl. Geochem. **61**, 233–247 (2015)
27. Miron, G.D., Kulik, D.A., Yan, Y., Tits, J., Lothenbach, B.: Extensions of CASH+ thermodynamic solid solution model for the uptake of alkali metals and alkaline earth metals in C–S–H. Cem. Concr. Res. **152**, 106667 (2022)
28. Myers, R.J., Bernal, S.A., Provis, J.L.: Phase diagrams for alkali-activated slag binders. Cem. Concr. Res. **95**, 30–38 (2017)
29. Provis, J.L., Lukey, G.C., van Deventer, J.S.J.: Do geopolymers actually contain nanocrystalline zeolites? A reexamination of existing results. Chem. Mater. **17**, 3075–3085 (2005)
30. Rowles, M.R., O'Connor, B.H.: Chemical and structural microanalysis of aluminosilicate geopolymers synthesized by sodium silicate activation of metakaolinite. J. Am. Ceram. Soc. **92**, 2354–2361 (2009)
31. Zuo, Y.: Experimental Study and Numerical Simulation of the Reaction Process and Microstructure Formation of Alkali-Activated Materials. Ph.D. thesis, Delft University of Technology (2019)
32. Chen, Y., de Lima, L.M., Li, Z., Ma, B., Lothenbach, B., Yin, S., Yu, Q., Ye, G.: Synthesis, solubility and thermodynamic properties of N–A–S–H gels with various target Si/Al ratios. Cem. Concr. Res. **180**, 107484 (2024)
33. Lothenbach, B., Bernard, E., Mäder, U.: Zeolite formation in the presence of cement hydrates and albite. Phys. Chem. Earth **99**, 77–94 (2017)
34. Ma, B., Lothenbach, B.: Thermodynamic study of cement/rock interactions using experimentally generated solubility data of zeolites. Cem. Concr. Res. **135**, 106149 (2020)
35. Ma, B., Lothenbach, B.: Synthesis, characterization, and thermodynamic study of selected K-based zeolites. Cem. Concr. Res. **148**, 106537 (2021)
36. Peys, A., Isteri, V., Yliniemi, J., Yorkshire, A.S., Lemougna, P.N., Utton, C., Provis, J.L., Snellings, R., Hanein, T.: Sustainable iron-rich cements: raw material sources and binder types. Cem. Concr. Res. **157**, 106834 (2022)
37. Ghazizadeh, S., Hanein, T., Provis, J.L., Matschei, T.: Estimation of standard molar entropy of cement hydrates and clinker minerals. Cem. Concr. Res. **136**, 106188 (2020)
38. Ye, H., Radlińska, A.: Quantitative analysis of phase assemblage and chemical shrinkage of alkali-activated slag. J. Adv. Concr. Technol. **14**, 245–260 (2016)
39. Zuo, Y., Nedeljković, M., Ye, G.: Coupled thermodynamic modelling and experimental study of sodium hydroxide activated slag. Constr. Build. Mater. **188**, 262–279 (2018)
40. Ke, X., Bernal, S.A., Provis, J.L., Lothenbach, B.: Thermodynamic modelling of phase evolution in alkali-activated slag cements exposed to carbon dioxide. Cem. Concr. Res. **136**, 106158 (2020)
41. Park, S., Lothenbach, B., Jang, J.G., Kim, H.-K., Lee, N.: Thermodynamic modeling and experimental study of carbonation of alkali-activated slag cements. ACS Sustain. Chem. Eng. **11**, 4049–4063 (2023)

42. Zuo, Y.: Effect of chloride salt on the phase evolution in alkali-activated slag cements through thermodynamic modelling. Appl. Geochem. **136**, 105169 (2022)
43. Zuo, Y.: Thermodynamic modeling of the phase evolution in alkali-activated slag cements with sulfate salt exposure. J. Am. Ceram. Soc. **105**, 18661 (2022)
44. Mundra, S., Prentice, D.P., Bernal, S.A., Provis, J.L.: Modelling chloride transport in alkali-activated slags. Cem. Concr. Res. **130**, 106011 (2020)
45. Chen, B., Zuo, Y., Zhang, S., de Lima Junior, L.M., Liang, X., Chen, Y., van Zijl, M.B., Ye, G.: Reactivity and leaching potential of municipal solid waste incineration (MSWI) bottom ash as supplementary cementitious material and precursor for alkali-activated materials. Constr. Build. Mater. **409**, 133890 (2023)
46. Shi, C.J., Day, R.L.: A calorimetric study of early hydration of alkali-slag cements. Cem. Concr. Res. **25**, 1333–1346 (1995)
47. Gebregziabiher, B.S., Thomas, R.J., Peethamparan, S.: Temperature and activator effect on early-age reaction kinetics of alkali-activated slag binders. Constr. Build. Mater. **113**, 783–793 (2016)
48. Gebregziabiher, B.S., Thomas, R., Peethamparan, S.: Very early-age reaction kinetics and microstructural development in alkali-activated slag. Cem. Concr. Comp. **55**, 91–102 (2015)
49. Gao, X., Yu, Q., Brouwers, H.: Reaction kinetics, gel character and strength of ambient temperature cured alkali activated slag–fly ash blends. Constr. Build. Mater. **80**, 105–115 (2015)
50. Zhang, Z., Provis, J.L., Wang, H., Bullen, F., Reid, A.: Quantitative kinetic and structural analysis of geopolymers. Part 2. Thermodynamics of sodium silicate activation of metakaolin. Thermochim. Acta **565**, 163–171 (2013)
51. Chithiraputhiran, S., Neithalath, N.: Isothermal reaction kinetics and temperature dependence of alkali activation of slag, fly ash and their blends. Constr. Build. Mater. **45**, 233–242 (2013)
52. Provis, J.L., van Deventer, J.S.J.: Geopolymerisation kinetics. 1. In situ energy-dispersive X-ray diffractometry. Chem. Eng. Sci. **62**, 2309–2317 (2007)
53. Provis, J.L., Walls, P.A., van Deventer, J.S.J.: Geopolymerisation kinetics. 3. Effects of Cs and Sr salts. Chem. Eng. Sci. **63**, 4480–4489 (2008)
54. Levenspiel, O.: Chemical Reaction Engineering, 3rd. Wiley, New York (1998)
55. Khawam, A., Flanagan, D.R.: Solid-state kinetic models: basics and mathematical fundamentals. J. Phys. Chem. B **110**, 17315–17328 (2006)
56. Fernández-Jiménez, A., Puertas, F.: Alkali-activated slag cements: kinetic studies. Cem. Concr. Res. **27**, 359–368 (1997)
57. Ginstling, A., Brounshtein, B.: Concerning the diffusion kinetics of reactions in spherical particles. J. Appl. Chem. USSR **23**, 1327–1338 (1950)
58. Provis, J.L.: On the use of the Jander equation in cement hydration modelling. RILEM Tech. Lett. **1**, 62–66 (2016)
59. Parrot LJK, D.C.: Prediction of cement hydration. Br. Ceram. Trans. **35**, 41–53 (1984)
60. Lapeyre, J., Han, T., Wiles, B., Ma, H., Huang, J., Sant, G., Kumar, A.: Machine learning enables prompt prediction of hydration kinetics of multicomponent cementitious systems. Sci. Rep. **11**, 3922 (2021)
61. Han, T., Ponduru, S.A., Cook, R., Huang, J., Sant, G., Kumar, A.: A deep learning approach to design and discover sustainable cementitious binders: strategies to learn from small databases and develop closed-form analytical models. Front. Mater. **8** (2022)
62. Faimon, J.: Oscillatory silicon and aluminum aqueous concentrations during experimental aluminosilicate weathering. Geochim. Cosmochim. Acta **60**, 2901–2907 (1996)
63. Provis, J.L., van Deventer, J.S.J.: Geopolymerisation kinetics. 2. Reaction kinetic modelling. Chem. Eng. Sci. **62**, 2318–2329 (2007)
64. Zhang, Z., Wang, H., Provis, J.L., Bullen, F., Reid, A., Zhu, Y.: Quantitative kinetic and structural analysis of geopolymers. Part 1. The activation of metakaolin with sodium hydroxide. Thermochim. Acta **539**, 23–33 (2012)
65. Yang, K., White, C.E.: Modeling the formation of alkali aluminosilicate gels at the mesoscale using coarse-grained Monte Carlo. Langmuir **32**, 11580–11590 (2016)

66. Yang, K., White, C.E.: Multiscale pore structure determination of cement paste via simulation and experiment: the case of alkali-activated metakaolin. Cem. Concr. Res. **137**, 106212 (2020)
67. Valentini, L.: Modeling dissolution-precipitation kinetics of alkali-activated Metakaolin. ACS Omega **3**, 18100–18108 (2018)
68. Bentz, D.P.: Three-dimensional computer simulation of Portland cement hydration and microstructure development. J. Am. Ceram. Soc. **80**, 3–21 (1997)
69. Bishnoi, S., Scrivener, K.L.: μic: a new platform for modelling the hydration of cements. Cem. Concr. Res. **39**, 266–274 (2009)
70. Breugel, K.V.: Simulation of Hydration and Formation of Structure in Hardening Cement-Based Materials. Ph.D., Delft University of Technology (1991)
71. Zuo, Y., Ye, G.: GeoMicro3D: A novel numerical framework for simulating the hydration and microstructure formation of alkali-activated materials. In: Ye, G. (ed.) Proceedings of Workshop on Concrete Modelling and Materials Behaviour in Honor of Professor Klaas van Breugel, RILEM, Delft, The Netherlands (2018)
72. Zuo, Y., Ye, G.: GeoMicro3D: a novel numerical model for simulating the reaction process and microstructure formation of alkali-activated slag. Cem. Concr. Res. **141**, 106328 (2021)
73. Xu, Z., Zuo, Y., Ye, G.: Lattice Boltzmann simulation of chloride transport in alkali-activated slag. In: Ye, G. (ed.) Proceedings of 4th International RILEM Conference on Microstructure Related Durability of cementitious Composites, RILEM, Delft, The Netherlands, Webinar (2021)
74. Ma, Q., Nanukuttan, S.V., Basheer, P.A.M., Bai, Y., Yang, C.: Chloride transport and the resulting corrosion of steel bars in alkali activated slag concretes. Mater. Struct. **49**, 3663–3677 (2016)
75. Dehghan, A., Peterson, K., Riehm, G., Herzog Bromerchenkel, L.: Application of X-ray microfluorescence for the determination of chloride diffusion coefficients in concrete chloride penetration experiments. Constr. Build. Mater. **148**, 85–95 (2017)
76. Richardson, I.G., Brough, A.R., Groves, G.W., Dobson, C.M.: The characterization of hardened alkali-activated blast-furnace slag pastes and the nature of the calcium silicate hydrate (C–S–H) phase. Cem. Concr. Res. **24**, 813–829 (1994)
77. Provis, J.L., Palomo, A., Shi, C.: Advances in understanding alkali-activated materials. Cem. Concr. Res. **78**, 110–125 (2015)
78. Król, M., Rożek, P., Chlebda, D., Mozgawa, W.: ATR/FT-IR studies of zeolite formation during alkali-activation of metakaolin. Solid State Sci. **94**, 114–119 (2019)
79. Bernard, O., Ulm, F.-J., Lemarchand, E.: A multiscale micromechanics-hydration model for the early-age elastic properties of cement-based materials. Cem. Concr. Res. **33**, 1293–1309 (2003)
80. Sanahuja, J., Dormieux, L., Chanvillard, G.: Modelling elasticity of a hydrating cement paste. Cem. Concr. Res. **37**, 1427–1439 (2007)
81. Königsberger, M., Pichler, B., Hellmich, C.: Multiscale poro-elasticity of densifying calcium-silicate hydrates in cement paste: an experimentally validated continuum micromechanics approach. Int. J. Eng. Sci. **147**, 103196 (2020)
82. Pichler, B., Hellmich, C.: Upscaling quasi-brittle strength of cement paste and mortar: a multi-scale engineering mechanics model. Cem. Concr. Res. **41**, 467–476 (2011)
83. Königsberger, M., Hlobil, M., Delsaute, B., Staquet, S., Hellmich, C., Pichler, B.: Hydrate failure in ITZ governs concrete strength: a micro-to-macro validated engineering mechanics model. Cem. Concr. Res. **103**, 77–94 (2018)
84. Pichler, C., Lackner, R., Mang, H.A.: A multiscale micromechanics model for the autogenous-shrinkage deformation of early-age cement-based materials. Eng. Fract. Mech. **74**, 34–58 (2007)
85. Königsberger, M., Irfan-ul-Hassan, M., Pichler, B., Hellmich, C.: Downscaling based identification of nonaging power-law creep of cement hydrates. J. Eng. Mech. **142**, 04016106 (2016)
86. Irfan-ul-Hassan, M., Königsberger, M., Reihsner, R., Hellmich, C., Pichler, B.: How water-aggregate interactions affect concrete creep: multiscale analysis. J. Nanomech. Micromech. **7**, 04017019 (2017)

87. Hlobil, M., Šmilauer, V., Chanvillard, G.: Micromechanical multiscale fracture model for compressive strength of blended cement pastes. Cem. Concr. Res. **83**, 188–202 (2016)
88. Göbel, L., Osburg, A., Pichler, B.: The mechanical performance of polymer-modified cement pastes at early ages: ultra-short non-aging compression tests and multiscale homogenization. Constr. Build. Mater. **173**, 495–507 (2018)
89. Göbel, L., Königsberger, M., Osburg, A., Pichler, B.: Viscoelastic behavior of polymer-modified cement pastes: insight from downscaling short-term macroscopic creep tests by means of multiscale modeling. Appl. Sci. **8**, 487 (2018)
90. Adessina, A., Ben Fraj, A., Barthélémy, J.-F., Chateau, C., Garnier, D.: Experimental and micromechanical investigation on the mechanical and durability properties of recycled aggregates concrete. Cem. Concr. Res. **126**, 105900 (2019)
91. Königsberger, M., Staquet, S.: Micromechanical multiscale modeling of ITZ-driven failure of recycled concrete: effects of composition and maturity on the material strength. Appl. Sci. **8**, 976 (2018)
92. Šmilauer, V., Hlaváček, P., Škvára, F., Šulc, R., Kopecký, L., Němeček, J.: Micromechanical multiscale model for alkali activation of fly ash and metakaolin. J. Mater. Sci. **46**, 6545–6555 (2011)
93. Das, S., Yang, P., Singh, S.S., Mertens, J.C., Xiao, X., Chawla, N., Neithalath, N.: Effective properties of a fly ash geopolymer: synergistic application of X-ray synchrotron tomography, nanoindentation, and homogenization models. Cem. Concr. Res. **78**, 252–262 (2015)
94. Fang, G., Zhang, M.: Multiscale micromechanical analysis of alkali-activated fly ash-slag paste. Cem. Concr. Res. **135**, 106141 (2020)
95. Jiang, D., Shi, C., Zhang, Z.: Recent progress in understanding setting and hardening of alkali-activated slag (AAS) materials. Cem. Concr. Comp. **134**, 104795 (2022)
96. Caron, R., Patel, R.A., Bogner, A., Dehn, F.: Multi-scale experimental investigation and analytical micro-mechanical modeling to determine Young's modulus of alkali-activated slag concrete. Constr. Build. Mater. **383**, 131272 (2023)